**Supplementary Information**

# Two-component latency distributions indicate two-step vesicular release at simple glutamatergic synapses

Miki et al.

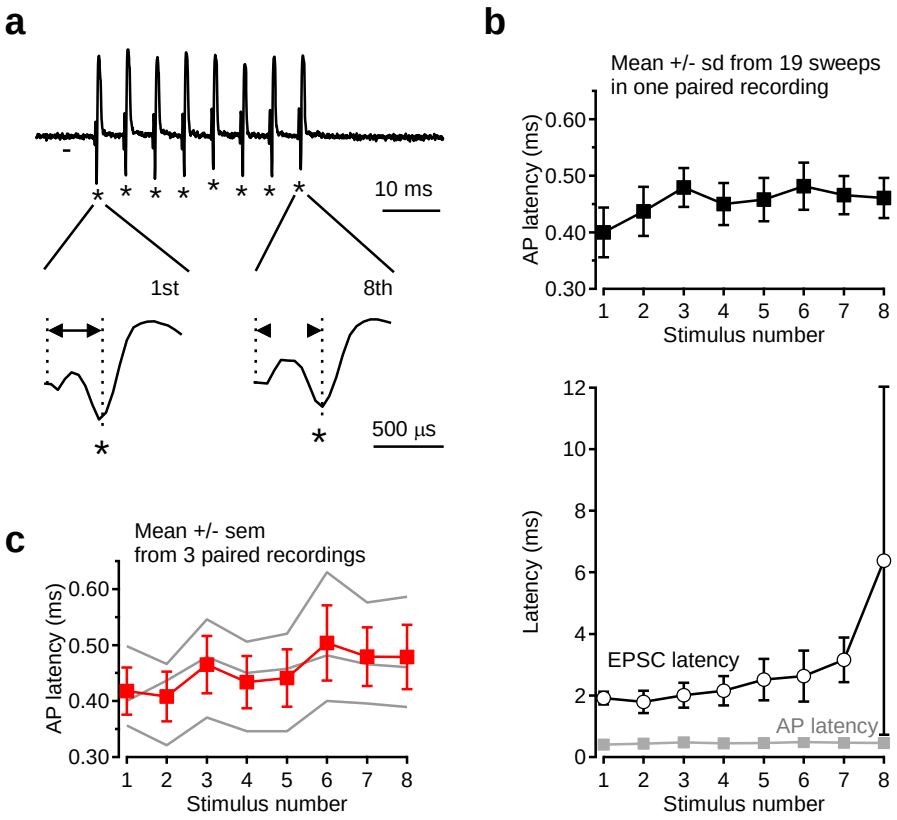


**Supplementary Figure 1**: Latencies of APs and release events in paired recordings
Latencies of APs and release events were detected by paired recording. Whole cell recording and cell-attached recording were performed in connected postsynaptic MLI and presynaptic GC soma.
**a**: A representative trace of cell-attached recording from a GC soma. 1 ms voltage steps were applied at 200 Hz. Peaks of AP-associated currents are shown by asterisks. These peaks correspond to the time point of maximum slope of the presynaptic AP[1]. We measured the time difference between the onset of voltage step and the peak of AP-associated currents (arrows in bottom panels).
**b**: Top, plot of AP latency (mean ± sd) vs. stimulus number, showing little jitter at a given stimulus number, and little variation of the mean latency during an AP train. Bottom, in contrast to AP latencies (grey squares, same as top panel), EPSC latencies (open symbols; mean ± sd) display significant jitter at each stimulus number, and their mean value increases with stimulus number. This plot displays the latencies of first events after each stimulation; an all-latency plot would display even broader scatter.
**c**: Group analysis of AP latencies from 3 paired recordings (mean ± sem). Gray lines indicate averages of individual paired recordings.

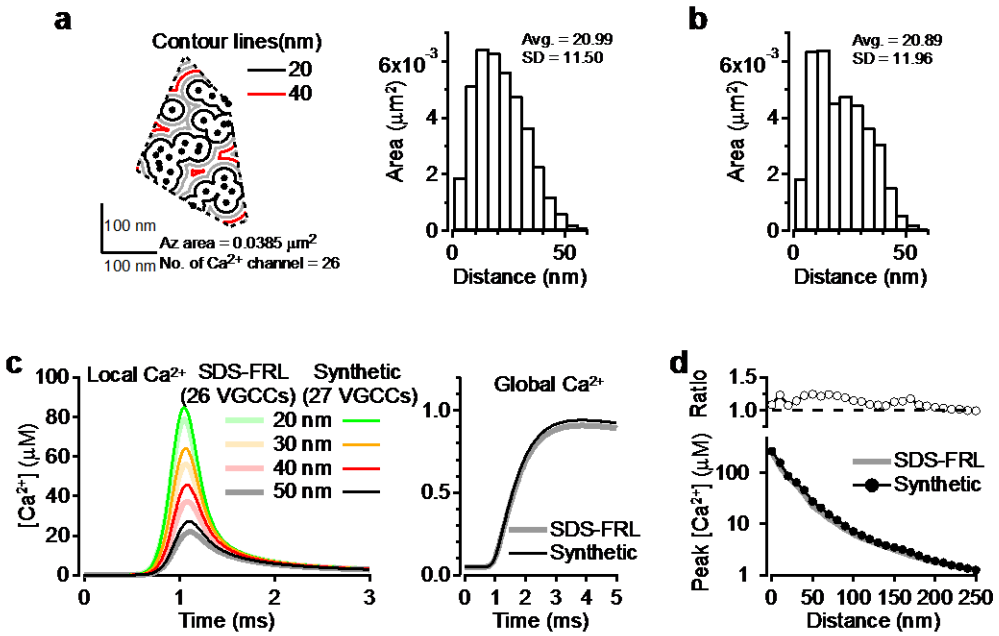


**Supplementary Figure 2**: $Ca^{2+}$ channel distributions in AZ

**a**: Left: A representative example of $Ca^{2+}$ channel labeling in a single PF-MLI AZ of a SDS-treated freeze fracture replica (SDS-FRL). Same data pool as in Miki et al.[2]. We chose an AZ that displayed an area close to the average (0.0427 μm²), and a number of $Ca^{2+}$ channel close to the average number corrected by labeling efficiency[2] (27). Contour lines show distances from nearest $Ca^{2+}$ channel. Dashed line shows the borders of the AZ area. Right: Histogram of area distribution of this representative data as a function of distance from nearest $Ca^{2+}$ channel in the AZ region.

**b**: Histogram of area distribution of the model AZ in Figure 1c. Note the similarity with the histogram in **a**. We used the slightly idealised version of Figure 1c in our simulations, because the 3-fold rotation symmetry of the distribution in Figure 1C facilitated the calculations of $Ca^{2+}$ diffusion.

**c**: Comparison of $[Ca^{2+}]$ waveforms calculated using the VGCC distribution in A and the model VGCC distribution of Fig. 1c.

**d**: Comparison of peak amplitudes of $[Ca^{2+}]$ waveforms between VGCC distribution from SDS-FRL data and model VGCC distribution. Upper: Ratio of peak $[Ca^{2+}]$ from model VGCC distribution to that from the SDS-FRL representative data. Lower: Peak $[Ca^{2+}]$ as a function of distance from nearest VGCC, for the two distributions.

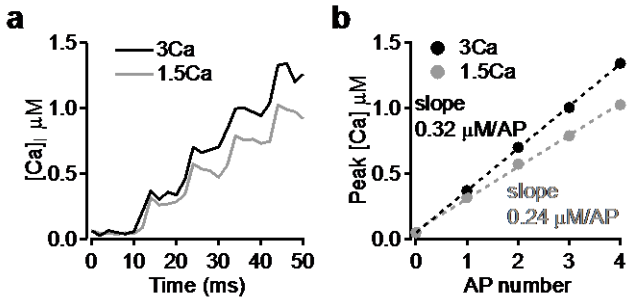


**Supplementary Figure 3**: 2-photon $Ca^{2+}$ imaging in PF varicosities
**a**: Time course of presynaptic intracellular [$Ca^{2+}$] in 1.5 and 3 mM extracellular [$Ca^{2+}$] conditions when applying 4 APs at 100 Hz.
**b**: Peak [$Ca^{2+}$] as a function of AP number in 1.5 and 3 mM extracellular [$Ca^{2+}$]. Linear fits have slopes of 0.24 and 0.32 μM/AP for 1.5 and 3 mM [$Ca^{2+}$] respectively. The difference between the value of 0.32 μM/AP in 3 mM extracellular [$Ca^{2+}$] obtained here and the value of 0.90 μM/AP used for [$Ca^{2+}$] simulation in Fig. 1d arises from the presence of exogenous buffers associated with the recording solution in the present experiments (see Methods).

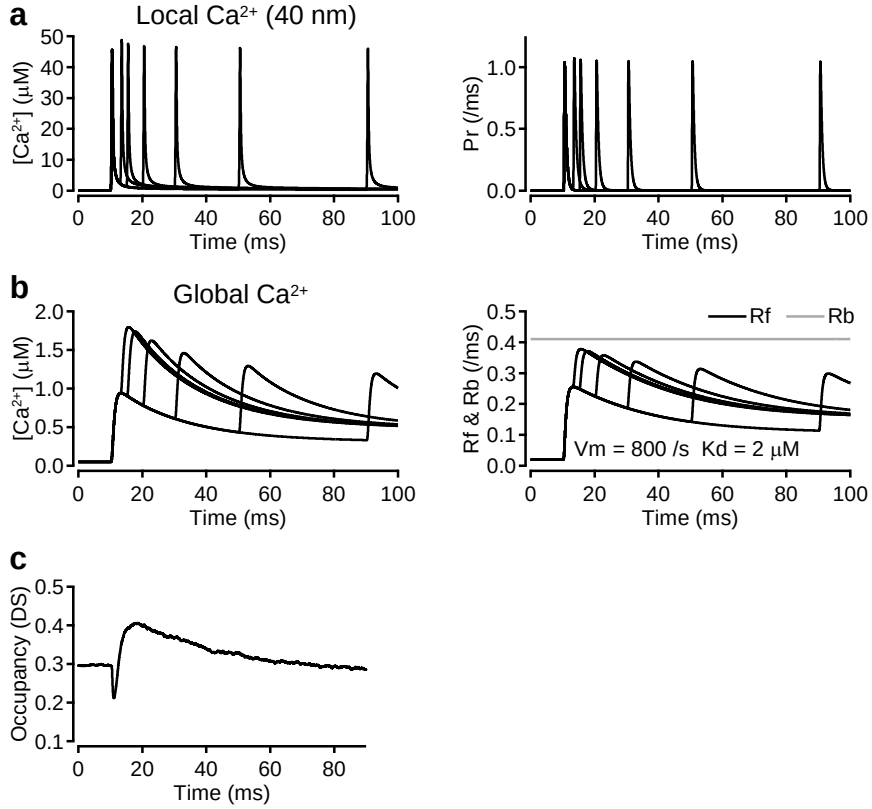


**Supplementary Figure 4**: Values of parameters for the simulation of paired-pulse experiments

**a**: Left panel: Local [$Ca^{2+}$] waves at 40 nm distance from $Ca^{2+}$ channel clusters for paired pulse stimulations with different inter-AP intervals. Right panel: $P_r$ were calculated from local [$Ca^{2+}$] waves using allosteric model with parameter values $k_{on}$ = 5 x $10^8$ $M^{-1}s^{-1}$, $k_{off}$ = 5000 $s^{-1}$, b = 0.75, g = 1500 $s^{-1}$, f = 31.3.

**b**: Left panel: Global [$Ca^{2+}$] waves for paired pulse stimulation with different intervals. Global [$Ca^{2+}$] was defined as the average of [$Ca^{2+}$] in x-y plane at z of 0.25 μm in the simulation bouton with a volume of 0.9(x) x 0.5(y) x 0.5(z) μm (Fig. 1c). Right panel: Replenishment rates from replacement site to docking site ($R_f$: forward rate, $R_b$: backward rate). $R_f$ is calculated using Michaelis-Menten kinetics based on the global [$Ca^{2+}$] profile shown in the left panel, assuming a maximum rate $V_m$ = 800/s and a $K_d$ of 2 μM. While this treatment is in conformity with previous modeling of $R_f$ (ref. 3), another option would be to calculate $R_f$ based on the quickly evolving local [$Ca^{2+}$] prevailing near the replacement site, at a distance of 45-90 nm from the plasma membrane, and to introduce a downstream rate limiting step to represent actual SV movement. We preferred the simpler first option to the second, potentially more relevant modeling because it contained a smaller number of free parameters.

**c**: Docking site occupancy (δ) displays a quick decrease followed by a rebound and an overshoot over the basal value within 5 ms. Then it slowly decays back to the resting state.

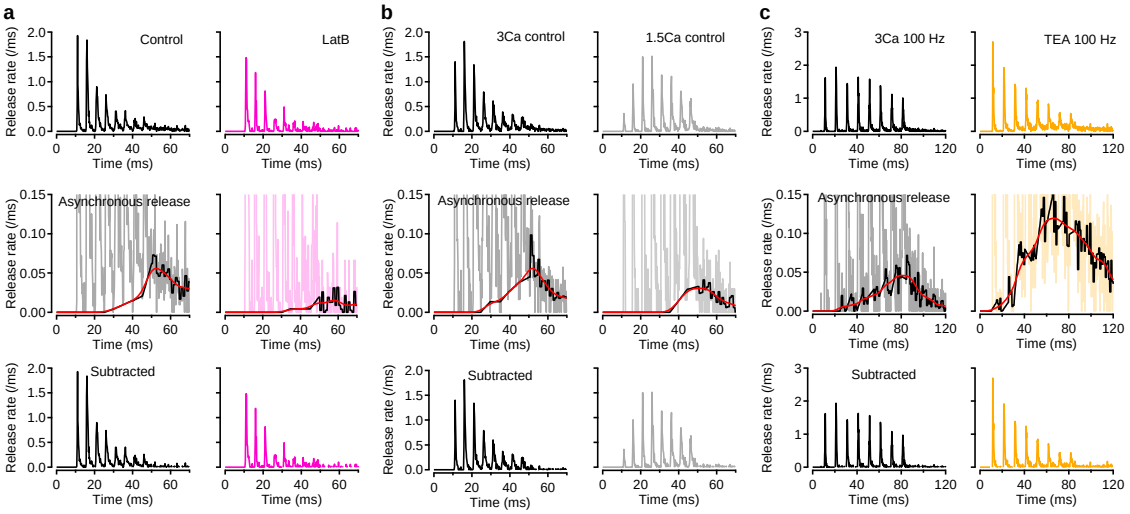


**Supplementary Figure 5**: Effects of various experimental manipulations on release rates during trains

Overall release rates (upper row) have been decomposed into a superslow component representing asynchronous release (middle row; expanded vertical scale) and a phasic component (lower row). To extract superslow component, we blanked release rates during 4 ms after every AP, filtered remaining points with a 5 points window (black trace in middle row) and performed smoothing (red trace in middle row).

**a**: Comparison between control synapses (3 mM external $[Ca^{2+}]$ and 200 Hz stimulation) and synapses pretreated with latrunculin B.

**b**: Comparison between 1.5 mM and 3 mM external $[Ca^{2+}]$ (200 Hz stimulation in each case).

**c**: Comparison between control recordings (3 mM external $[Ca^{2+}]$ and 100 Hz stimulation) and test recordings obtained after adding 1 mM TEA to increase release probability.

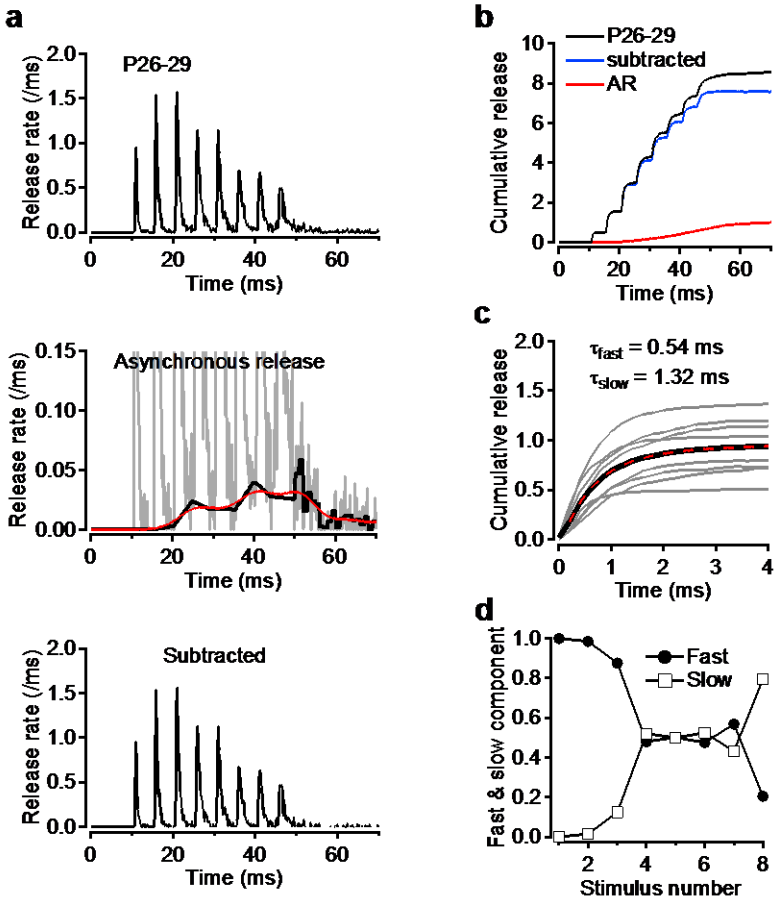


**Supplementary Figure 6**: Time course of fast, slow and asynchronous release during AP trains in 4 weeks old rats

**a**: Average release rate (per ms and per simple synapse; 3mM external [$Ca^{2+}$] and 200 Hz stimulation; n = 10 experiments). Middle panel: Expanded vertical scale highlighting asynchronous release. Lower panel: Average release rate after subtracting asynchronous release from original average release rate.

**b**: Cumulative latency counts.

**c**: Superimposed cumulative latency distributions for each AP stimulation during 8-AP train. Average traces of 8-AP responses (thick black curve) is fitted with a double exponential (red) with indicated $\tau_{fast}$ and $\tau_{slow}$ values.

**d**: Relative contributions of $\tau_{fast}$ and $\tau_{slow}$ component as a function of stimulus number.

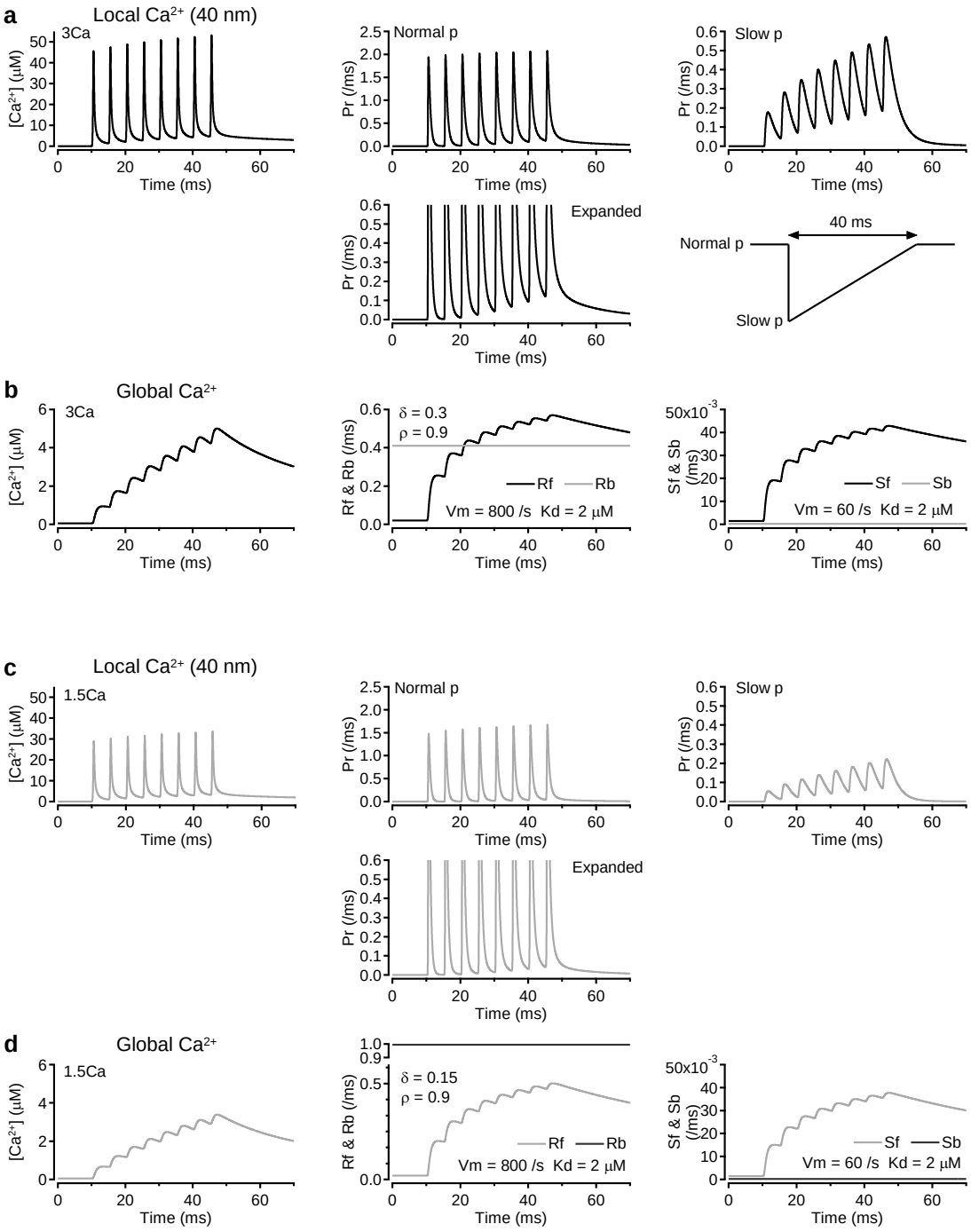


**Supplementary Figure 7**: Parameter values for the simulation of 8-pulse experiments in 3 and 1.5 mM external $[Ca^{2+}]$ conditions

**a**: Average $[Ca^{2+}]_i$ wave at a 40-nm distance from the nearest $Ca^{2+}$ channels for 200 Hz stimulation in 3 mM external $[Ca^{2+}]$ condition (3Ca; left). $P_r$ was calculated from local $[Ca^{2+}]_i$ using the standard allosteric model ($k_{on}$ = 5 x $10^8$ $M^{-1}s^{-1}$, $k_{off}$ = 5000 $s^{-1}$, b = 0.75, $\gamma$ = 2800 $s^{-1}$, f = 31.3 ; upper middle). The bottom middle panel shows a vertically expanded plot of $P_r$, illustrating the widening and accumulation of late

release rate as a function of stimulus number. Slow $P_r$ was calculated starting from the local $[Ca^{2+}]_i$ profile shown in the left panel, using modified parameter values of the allosteric model ($k_{on}$ = 5 x $10^7$ $M^{-1}s^{-1}$, $k_{off}$ = 2000 $s^{-1}$, b = 0. 5, $\gamma$ = 2000 $s^{-1}$, f = 31.3 ; right). The lower right panel shows a diagram illustrating the return from high $P_r$ release to low $P_r$ release, where each parameter linearly changes from its high $P_r$ value to its low $P_r$ value over a period of 40 ms.

**b**: Left, global $[Ca^{2+}]_i$ wave for 3Ca condition. Middle, $R_f$ was calculated from global $[Ca^{2+}]_i$ wave using a Michaelis-Menten reaction having a maximum speed ($V_m$) of 800 $s^{-1}$ and a dissociation constant ($K_d$) of 2 μM. $R_b$ value was set such that the occupancies of docking site ($\delta$ = 0.3) and replacement site ($\rho$ = 0.9) were kept constant at the resting state assuming $[Ca^{2+}]_{rest}$ of 50 nM. Right, $S_f$ was calculated from global $[Ca^{2+}]_i$ wave using a Michaelis-Menten reaction having $V_m$ = 60 $sec^{-1}$ and $K_d$ = 2 μM. $S_b$ value was set such that the occupancy of replacement site ($\rho$ = 0.9) was kept constant at the resting state.

**c**: Average $[Ca^{2+}]_i$ wave at 40-nm distance from the nearest $Ca^{2+}$ channels for 200 Hz stimulation in 1.5 mM external $[Ca^{2+}]$ condition (1.5Ca; left). $P_r$ was calculated from local $[Ca^{2+}]_i$ with standard allosteric model parameters ($k_{on}$ = 5 x $10^8$ $M^{-1}s^{-1}$, $k_{off}$ = 5000 $s^{-1}$, b = 0.75, $\gamma$ = 2800 $s^{-1}$, f = 31.3 ; upper middle). Expanded $P_r$ plot displays signifcantly less widening and accumulation of late release rates compared to 3Ca (bottom middle panel; compare with A). Slow $P_r$ was calculated from local $[Ca^{2+}]_i$ with the modified allosteric model ($k_{on}$ = 5 x $10^7$ $M^{-1}s^{-1}$, $k_{off}$ = 2000 $M^{-1}s^{-1}$, b = 0. 5, g = 2000 $s^{-1}$, f = 31.3), showing a marked decrease of the slow release rate compared to 3Ca (right panel).

**d**: Left, global $[Ca^{2+}]_i$ wave for 1.5Ca. Middle, $R_f$ was calculated by global $[Ca^{2+}]_i$ wave using a Michaelis-Menten reaction having a maximum speed ($V_m$) of 800 $s^{-1}$ and a dissociation constant ($K_d$) of 2 μM. $R_b$ value was set such that the occupancies of docking site ($\delta$ = 0.15) and replacement site ($\rho$ = 0.9) were kept constant at the resting state assuming $[Ca^{2+}]_{rest}$ of 50 nM. Right, $S_f$ was calculated from global $[Ca^{2+}]_i$ wave using a Michaelis-Menten reaction having $V_m$ = 60 $sec^{-1}$ and $K_d$ = 2 μM. $S_b$ value was set such that the occupancy of replacement site ($\rho$ = 0.9) was kept constant at the resting state.

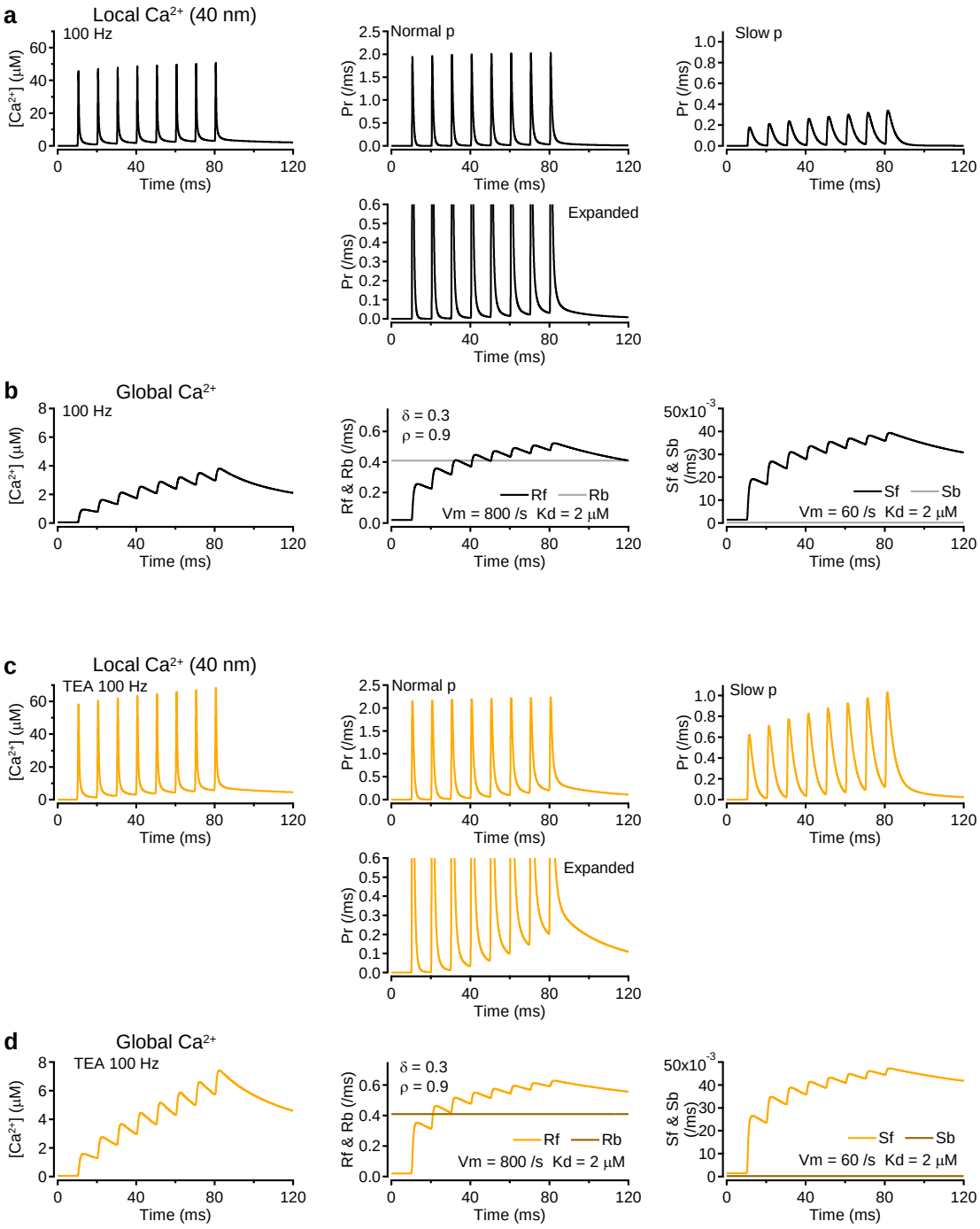


**Supplementary Figure 8**: Parameter values for the simulation of 100-Hz 8-pulse experiments in control and in TEA

**a**: Average $[Ca^{2+}]_i$ wave at a 40-nm distance from the nearest $Ca^{2+}$ channels for 100 Hz stimulation in 3 mM external $[Ca^{2+}]$ condition (3Ca; left). $P_r$ was calculated on the basis of local $[Ca^{2+}]_i$ using the allosteric model ($k_{on}$ = 5 x $10^8$ $M^{-1}s^{-1}$, $k_{off}$ = 5000 $s^{-1}$, b = 0.75, $\gamma$ = 2800 $s^{-1}$, f = 31.3 ; upper middle). The bottom middle panel shows a vertically expanded plot of $P_r$, showing less slowing and less accumulation than at

200 Hz (compare with Supplementary Fig. 6A). As before slow $P_r$ was calculated starting from the local $[Ca^{2+}]_i$ profile shown in the left panel, using the modified allosteric model ($k_{on}$ = 5 x $10^7$ $M^{-1}s^{-1}$, $k_{off}$ = 2000 $s^{-1}$, b = 0. 5, $\gamma$ = 2000 $s^{-1}$, f = 31.3; right).

**b**: Left, global $[Ca^{2+}]_i$ wave for 3Ca condition at 100 Hz. Middle, $R_f$ was calculated from global $[Ca^{2+}]_i$ wave using a Michaelis-Menten reaction having a maximum speed ($V_m$) of 800 $s^{-1}$ and a dissociation constant ($K_d$) of 2 μM. $R_b$ value was set such that the occupancies of docking site ($\delta$ = 0.3) and replacement site ($\rho$ = 0.9) were kept constant at the resting state assuming $[Ca^{2+}]_{rest}$ of 50 nM. Right, $S_f$ was calculated from global $[Ca^{2+}]_i$ wave using a Michaelis-Menten reaction having $V_m$ = 60 $sec^{-1}$ and $K_d$ = 2 μM. $S_b$ value was set such that the occupancy of replacement site ($\rho$ = 0.9) was kept constant at the resting state.

**c**: Average $[Ca^{2+}]_i$ wave at 40-nm distance from the nearest $Ca^{2+}$ channels for 100 Hz stimulation in 3 mM external $[Ca^{2+}]$ and in the presence of 1 mM TEA (left). $P_r$ was calculated on the basis of local $[Ca^{2+}]_i$ with standard allosteric model parameters ($k_{on}$ = 5 x $10^8$ $M^{-1}s^{-1}$, $k_{off}$ = 5000 $s^{-1}$, b = 0.75, $\gamma$ = 2800 $s^{-1}$, f = 31.3 ; upper middle). Expanded $P_r$ plot displays significantly more widening and accumulation of late release rates compared to 3Ca (bottom middle panel; compare with A). Slow $P_r$ was calculated by local $[Ca^{2+}]_i$ with the modified allosteric model ($k_{on}$ = 5 x $10^7$ $M^{-1}s^{-1}$, $k_{off}$ = 2000 $s^{-1}$, b = 0. 5, $\gamma$ = 2000 $s^{-1}$, f = 31.3), showing a marked increase of the slow release rate compared to 3Ca (right panel).

**d**: Left, global $[Ca^{2+}]_i$ wave for 3Ca plus TEA condition. Center, $R_f$ was calculated from global $[Ca^{2+}]_i$ wave using a Michaelis-Menten reaction having a maximum speed ($V_m$) of 800 $s^{-1}$ and a dissociation constant ($K_d$) of 2 μM. $R_b$ was set such that the occupancies of docking site ($\delta$ = 0.3) and replacement site ($\rho$ = 0.9) were kept constant at the resting state assuming $[Ca^{2+}]_{rest}$ of 50 nM. Right, $S_f$ was calculated from global $[Ca^{2+}]_i$ wave using a Michaelis-Menten reaction having $V_m$ = 60 $sec^{-1}$ and $K_d$ = 2 μM. $S_b$ value was set such that the occupancy of replacement site ($\rho$ = 0.9) was kept constant at the resting state.

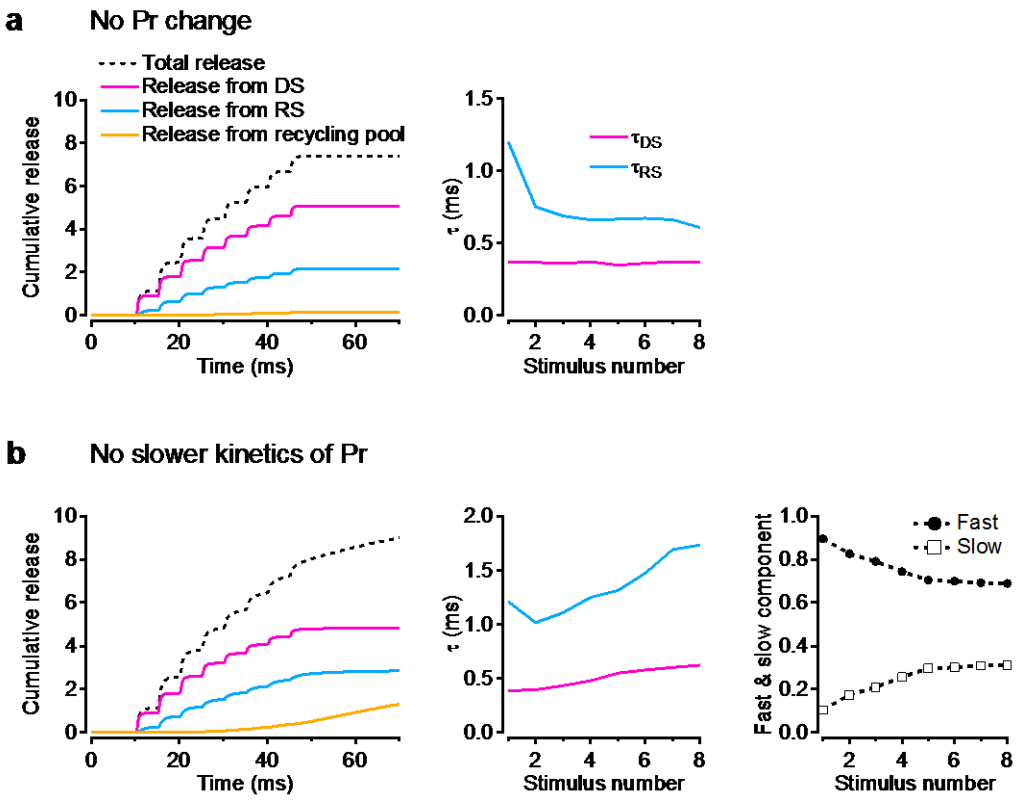


**Supplementary Figure 9**: Release simulations for train stimulus without changes in $[Ca^{2+}]_i$ profile or without shift to slower $P_r$

Kinetics of total cumulative release and cumulative release from docking site (DS), replacement site (RS), and recycling pool.

**a**: Monte Carlo simulation was performed using same $P_r$ among all stimulations as that for single stimulation in 3 mM external $[Ca^{2+}]$ simulation. Left, total cumulative release and cumulative release from 3 different resources are shown: total (black), DS (red), RS (blue), and recycling pool (orange). Right, $\tau$ values for kinetics of release from DS (red) and RS (blue) were derived from fitting the cumulative release in each stimulation with a single exponential curve.

**b**: Monte Carlo simulation was performed without using slower $P_r$ following previous release. Left, total cumulative release and cumulative release from 3 different resources are shown in black for total, red for DS, blue for RS, and orange for recycling pool. Middle, $\tau$ values for kinetics of release from DS (red) and RS (blue) were derived from fitting the cumulative release in each stimulation with a single exponential curve. Total cumulative release of each response was fitted with a double exponential curve having $\tau_{fast}$ of 0.49 ms and $\tau_{slow}$ of 1.87 ms, providing fast and slow component amplitudes as a function of stimulus number (right).

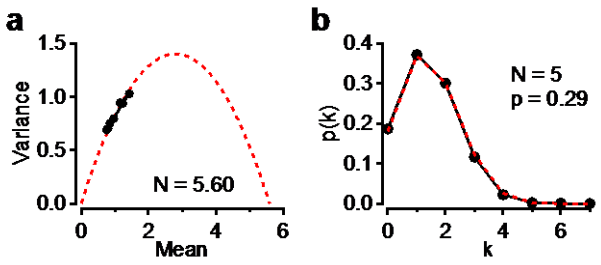


**Supplementary Figure 10**: Binomial statistical analysis of the number of release events in 3 mM external [$Ca^{2+}$] simulation

**a**: The mean and variance of the number of events were determined in a 5-ms period after individual stimulations in 3 mM external [$Ca^{2+}$] simulation. The resulting curve can be fitted with a parabola indicating a release site number N = 5.60 (dashed curve).

**b**: The probability distribution p(k) to observe k events is displayed for the second stimulus in A. The binomial model approximates the plot from the simulation (dashed line; N = 5; mean probability P = 0.29).

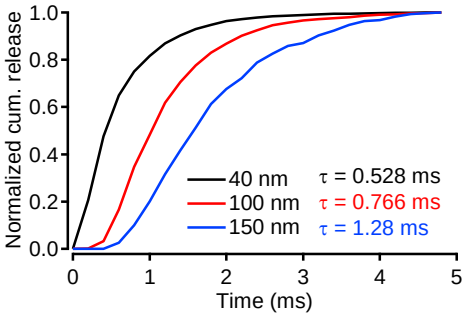


**Supplementary Figure 11**: Simulated latency distributions depending on the distance between release sites and $Ca^{2+}$ channel clusters

$Ca^{2+}$ waves at 40-, 100-, and 150-nm from the perimeter of $Ca^{2+}$ channel cluster were used to simulate cumulative release. The cumulative release curves were normalized and fitted with a single exponential to estimate release latencies. The time constant $\tau$ was 0.528, 0.766, and 1.28 ms for 40, 100, and 150 nm, respectively.

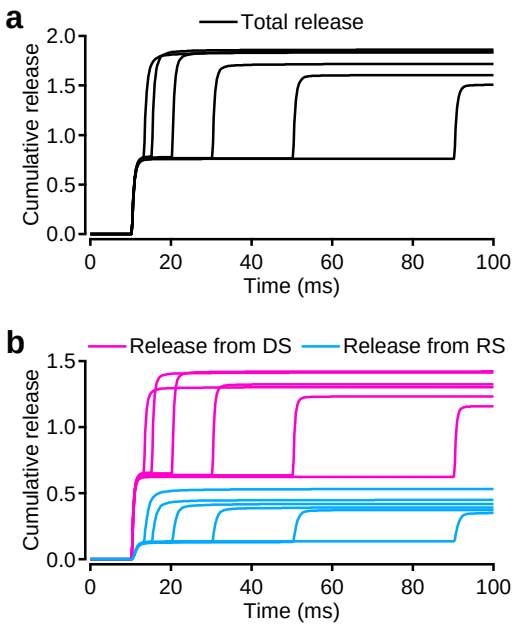


**Supplementary Figure 12**: Monte Carlo simulations for paired pulse experiments
**a**: Total cumulative release for paired stimulations with 6 different intervals.
**b**: Cumulative releases for SVs originating from DS and RS are shown in red and blue, respectively. This plot shows a marked increase in the relative contribution of SVs coming from RS for the second stimulation compared to the first.

**Supplementary Table 1**: Parameters for simulations of $[Ca^{2+}]$ diffusion

| Simulation Parameters | value | units | Reference |
|---|---|---|---|
| | | | |
| Simulation volume (bouton size) *x-y-z* | 0.9 - 0.5 - 0.5 | μm | Modified from Hillman & Chen[4] |
| Simulation voxel size | 10 | nm | |
| Time step for Ca simulation | 0.0303 | μs | |
| | | | |
| ***$Ca^{2+}$ entry per single AP*** | | | |
| Maximal single channel current | 0.2 (3 mM Ca)<br>0.14 (1.5 mM Ca) | pA | Calculated from Weber et al.[5] and Li et al.[6] for 3 mM Ca<br>Adjusted to Ca imaging data for 1.5 mM Ca |
| FWHM of $Ca^{2+}$ entry | 0.34 (control)<br>0.68 (TEA) | ms | Sabatini & Regehr[7] for control.<br>Adjusted to Ca imaging data for TEA. |
| Diffusion coefficient | 0.22 | $\mu m^2\ ms^{-1}$ | Allbritton et al.[8] |
| | | | |
| ***Basal $Ca^{2+}$ concentration*** | 50 | nM | Sabatini & Regehr[7] |
| ***$Ca^{2+}$ extrusion*** | 0.9 | $ms^{-1}$ | Helmchen et al.[9] |
| | | | |
| | | | |
| ***Endogenous fixed buffer properties*** | | | |
| $k_{on}$ | 200 | $mM^{-1}ms^{-1}$ | Sabatini & Regehr[7] |
| $k_{off}$ | 10 | $ms^{-1}$ | |
| Concentration | 2 | mM | |
| | | | |
| ***ATP calcium binding properties*** | | | |
| $k_{on}$ | 500 | $mM^{-1}ms^{-1}$ | Naraghi & Neher[10] |
| $k_{off}$ | 100 | $ms^{-1}$ | |
| Diffusion coefficient | 0.22 | $\mu m^2\ ms^{-1}$ | |
| Free concentration | 0.2 | mM | Modified from Nakamura et al.[11] |
| | | | |
| ***Calretinin*** | | | |
| T site $k_{on}$ | 1.8 | $mM^{-1}ms^{-1}$ | Faas et al.[12] |
| T site $k_{off}$ | 0.053 | $ms^{-1}$ | |
| R site $k_{on}$ | 310 | $mM^{-1}ms^{-1}$ | |
| R site $k_{off}$ | 0.02 | $ms^{-1}$ | |
| Diffusion coefficient | 0.02 | $\mu m^2\ ms^{-1}$ | |
| Concentration | 0.1 | mM | See Methods |

## Supplementary References


1. Alcami, P., Franconville, R., Llano, I. & Marty, A. Measuring the firing rate of high resistance neurons with cell-attached recording. *J. Neurosci.* **32**, 3118–3130 (2012).
2. Miki, T., Kaufmann, W., Malagon, G., Gomez, L., Tabuchi, K., Watanabe, M., Shigemoto, R., & Marty, A. Numbers of presynaptic $Ca^{2+}$ channel clusters match those of functionally defined vesicular docking sites in single central synapses. *Proc. Nat. Acad. Sci. USA.* **114**, E5246–E5255 (2017).
3. Neher, E., & Sakaba, T. Multiple roles of calcium ions in the regulation of neurotransmitter release. *Neuron* **59**, 861–870 (2008).
4. Hillman, D. E., & Chen, S. Compensation in the number of presynaptic dense projections and synaptic vesicles in remaining parallel fibers following cerebellar lesions. *J. Neurocytol.* **14**, 673–687 (1985).
5. Weber, A. M., Wong, F. K., Tufford, A. R., Schlichter, L. C., Matveev, V., & Stanley, E. N-type $Ca^{2+}$ channels carry the largest current: implications for nanodomains and transmitter release. *Nat. Neurosci.* **13**, 1348–1350 (2010).
6. Li, L., Bischofberger, J., & Jonas, P. Differential gating and recruitment of P/Q-, N-, and R-type $Ca^{2+}$ channels in hippocampal mossy fiber boutons. *J. Neurosci.* **27**, 13420–13429 (2007).
7. Sabatini, B., & Regehr, W. G. Optical measurement of presynaptic calcium currents. *Biophys. J.* **74**, 1549–1583 (1998).
8. Allbritton, N. L., Meyer, T., & Stryer, L. Range of messenger action of calcium ion and inositol 1,4,5-trisphosphate. *Science* **258**, 1812–1815 (1992).
9. Helmchen, F., Borst, J. G., & Sakmann, B. Calcium dynamics associated with a single action potential in a CNS presynaptic terminal. *Biophys. J.* **72**, 1458–1471 (1997).
10. Naraghi, M., & Neher, E. Linearized buffered $Ca^{2+}$ diffusion in microdomains and its implications for calculation of $[Ca^{2+}]$ at the mouth of calcium channel. *J. Neurosci.* **17**, 6961–6973 (1997).
11. Nakamura, Y., Harada, H., Kamasawa, N., Matsui, K., Rothman, J. S., Shigemoto, R., Silver, R. A., DiGregorio, D. A., & Takahashi, T. Nanoscale distribution of presynaptic $Ca^{2+}$ channels and its impact on vesicular release during development. *Neuron* **85**, 145–158 (2015).
12. Faas, G. C., Schwaller, B., Vergara, J. L., & Mody, I. Resolving the fast kinetics of cooperative binding: $Ca^{2+}$ buffering by calretinin. *PLos Biol.* **5**, e311 (2007).